ACS SyntheticBiology

pubs.acs.org/synthbio Research Article

Comprehensive Parameter Space Mapping of Cell Cycle Dynamics under Network Perturbations

Published as part of ACS Synthetic Biology virtual special issue "Quantitative Synthetic Biology".

Zhengda Li, Shiyuan Wang, Meng Sun, Minjun Jin, Daniel Khain, and Qiong Yang*

Cite This: *ACS Synth. Biol.* 2024, 13, 804–815 Read Online

ACCESS | Metrics & More | Article Recommendations | Supporting Information

ABSTRACT: Studies of quantitative systems and synthetic biology have extensively utilized models to interpret data, make predictions, and guide experimental designs. However, models often simplify complex biological systems and lack experimentally validated parameters, making their reliability in perturbed systems unclear. Here, we developed a droplet-based synthetic cell system to continuously tune parameters at the single-cell level in multiple dimensions with full dynamic ranges, providing an experimental framework for global parameter space scans. We systematically perturbed a cell-cycle oscillator centered on cyclin-dependent kinase (Cdk1), enabling comprehensive mapping of period landscapes in response to network perturbations. The data allowed us to challenge existing models and refine a new model that matches the observed response. Our analysis demonstrated that Cdk1 positive feedback inhibition restricts the cell cycle frequency range, confirming model predictions; furthermore, it revealed new cellular responses to the inhibition of the Cdk1-counteracting phosphatase PP2A: monomodal or bimodal distributions across varying inhibition levels, underscoring the complex nature of cell cycle regulation that can be explained by our model. This comprehensive perturbation platform may be generalizable to exploring other complex dynamic systems.

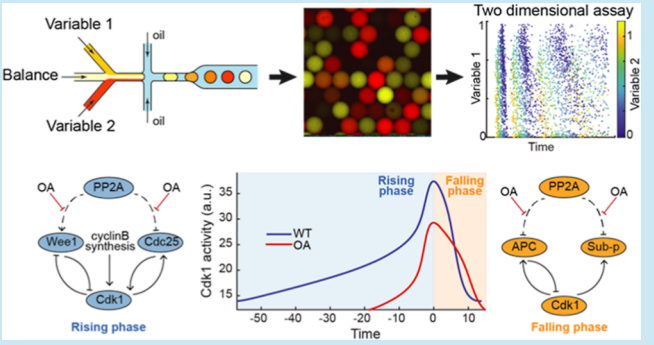

KEYWORDS: *tunability, cell cycle oscillation, positive feedback loops, droplet microfluidics, synthetic cells*

1. INTRODUCTION

Most multicellular life starts with a series of rapid synchronous embryonic cell cycles. Unlike somatic cells that undergo four distinct cell cycle phases, early embryonic cells lack G1/G2 gap phases, checkpoint machinery, or transcriptional activity, and oscillate between the S phase and M phase until zygotic genome activation (ZGA).[1−3] Nonetheless, the basic components of the oscillatory networks are shared among early embryonic and somatic cell cycles and are evolutionarily conserved across almost all eukaryotic species.

Pioneering research using *Xenopus* egg cytoplasmic extract has uncovered key molecules and regulatory mechanisms conserved from yeast to humans.[4] In the core circuitry, the cyclin B1 protein, upon synthesis, binds to Cdk1 to form a protein complex, cyclin B1-Cdk1. The activation of cyclin B1-Cdk1 facilitated through two coupled auxiliary positive feedback loops, Cdk1/Cdc25/Wee1, drives mitotic entry and activates the E3 ubiquitin ligase, anaphase-promoting complex, or cyclosome (APC/C), which in turn marks the cyclin B1 for degradation and deactivates Cdk1, completing a negative feedback loop and resulting in mitotic exit (Figure 1A).

In theory, a negative feedback loop alone can generate oscillations. In reality, however, cell cycle networks involve many more complicated regulatory components that form coupled positive and negative feedback loops.[5] Researchers have constructed mathematical models, both simple and complex, to understand the role of these regulatory circuits in cell cycle behaviors observed in experiments. Novak and Tyson[6] and Thron[7] first proposed the role of the Cdk1/Cdc25/Wee1 positive feedback system as a bistable trigger for mitotic entry, which was later confirmed by experiments.[8] Novak and Tyson constructed a detailed mass action model with 10 equations[9] (henceforth referred to as the "Novak–Tyson-full" model). Following that initial work, they then simplified it into a two-equation model based on Goldbeter–Koshland kinetics[10] (henceforth referred to as the "Novak–

Received: October 16, 2023
Revised: February 14, 2024
Accepted: February 16, 2024
Published: February 29, 2024

https://doi.org/10.1021/acssynbio.3c00631
ACS Synth. Biol. 2024, 13, 804–815

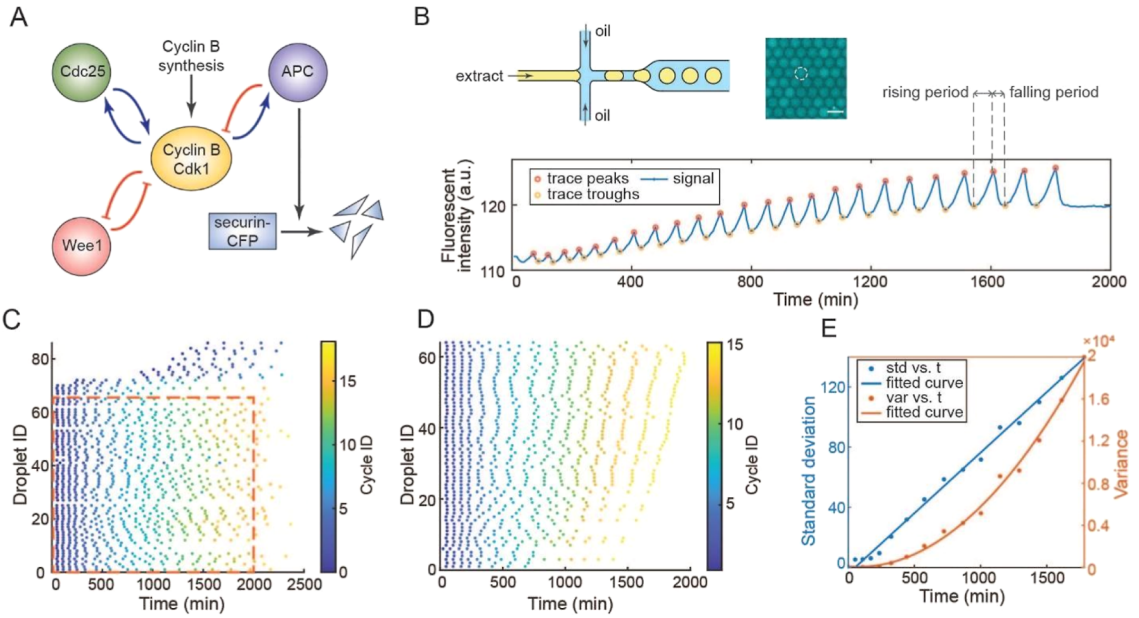

Figure 1. High-throughput microfluidic platform to study*Xenopus* embryonic cell cycle dynamics. (A) Schematic view of the mitotic circuit with a positive-to-negative feedback loop design. Securin-CFP is used as the cell cycle indicator. (B) Top left: schematic view of a single-channel microfluidic device. Top right: a fluorescent image of droplets with securin-CFP. Scale bar: 100 μm. Bottom: temporal fluorescent profile of an example droplet. Peaks and troughs are selected by custom MATLAB scripts and then manually corrected. (C) Raster plot of mitotic oscillations over time. Each dot represents one peak in the fluorescent profile of one droplet placed at the time of the peak. (D) Postprocessing raster plot of the same data set. Incomplete tracks are discarded, and the remaining droplets (the selected area from the left figure) are sorted by average period length and reassigned droplet IDs. All points beyond the 15th cycle are also discarded. (E) Standard deviation and variance of peak times against time. Each point represents all of the droplets with the same cycle ID.

Tyson-2equ" model). Yang and Ferrell also developed a two-equation model using Hill function-based rate equations[11] (henceforth referred to as "Yang−Ferrell" model). This model highlighted the important role of the hypersensitive response of APC/C to Cdk1 and a sufficient time delay in the robust cell cycle oscillations, which were verified experimentally. Modeling work by Tsai and Ferrell also predicted that the interlinked positive and negative feedback promotes robust oscillation and expands the frequency range (i.e., tunability) of cell cycles.[12] Remarkably, cell cycle modeling also predicted a significant role of phosphatase(s) in cell cycle regulation before the discovery of the importance of the protein phosphatase 2A (PP2A).[10]

Despite these models playing a significant role in advancing the understanding of cell cycle regulation principles and informing experimental design, there are key challenges for all current models. First, even the simplest models may contain many unknown parameters that are challenging to estimate. Experimentally measuring parameters is labor-intensive and can yield inconsistent results across different laboratories and batches. Direct measurements from experiments are impractical for some highly abstract parameters in simplified models. Second, to reduce complex biological systems, models often have assumptions about chemical reactions that are not necessarily realistic. For instance, the three aforementioned cell-cycle models used different rate functions and simplified the Cdk1 network differently. Therefore, the effectiveness of these models under altered conditions is questionable. Lastly, additional regulatory networks of the cell cycle have been discovered in recent years, and the classical models need to be modified to incorporate these new circuits. Notably, while previous models only considered positive feedback loops involving Wee1 and Cdc25, recent research suggests the need to include additional positive feedback regulation between Cdk1 and its counteracting phosphatase, especially PP2A.[13−16] Yet, there has not been a systematic study on how PP2A affects embryonic cell cycle dynamics.

An important step toward addressing these challenges is to systematically quantify cell cycle dynamics and map the entire oscillation landscape of the network under global parameter perturbations. Compared to measuring parameters individually, such a fine-grained multidimensional data set enables more reliable parameter estimation by global fitting and hence provides better constraints of models for their efficacy evaluation.

To this end, we developed a programmable multichannel microfluidic platform that generates water-in-oil emulsion droplets of precise size and composition, allowing for high-throughput, multivariable tuning of biochemical systems that can be encapsulated in the droplets. Using this technique, we systematically scrutinized cell cycle dynamics in droplets encapsulating *Xenopus* egg extracts under perturbations of cyclin B1, Wee1, and the recently identified PP2A circuit, either individually or in combination. The cell-free extracts provide an exceptional system for such perturbation analysis as it permits the direct incorporation of various cell-impermeable molecules such as mRNAs, proteins, and sensors. We further examined the behavior of classical cell cycle models under these combinatory perturbations and compared them to our experimental results. To incorporate the PP2A perturbation data, we constructed a cell cycle model including the PP2A circuit based on the Yang−Ferrell model and identified the parameter space that supports the free-running oscillation. Modeling the experimental perturbation responses offers insights into how this newly incorporated PP2A circuit

https://doi.org/10.1021/acssynbio.3c00631
ACS Synth. Biol. 2024, 13, 804−815

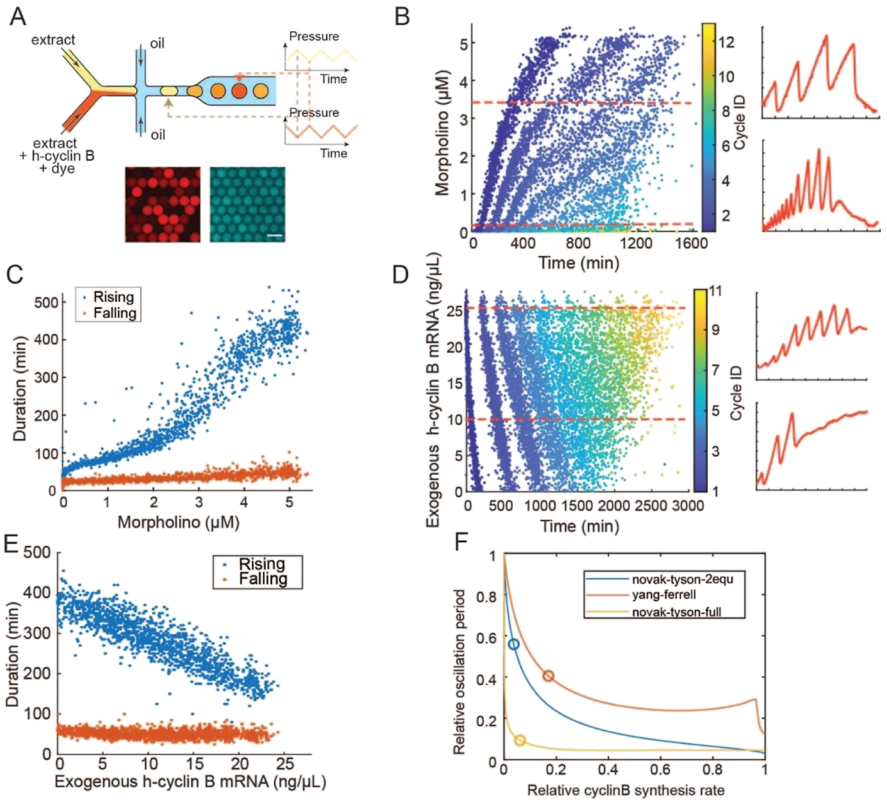

Figure 2. Frequency tuning with mRNA and morpholino. (A) Top: schematic view of a two-channel microfluidic device. Fluorescent dye is coadded with cyclin B mRNA to index concentration. Bottom: fluorescent images of droplets generated. Bottom left: fluorescent dye. Bottom right: securin-CFP. Scale bar 100 μm. (B) Left: Raster plot of droplets with varying morpholino concentrations. Right: fluorescent profiles of two example droplets with different morpholino concentrations, indicated by dashed lines in the left figure. (C) Rising and falling periods vs morpholino concentration. Only the first cycle periods are included in the figure for clarity. (D) Left: Raster plot of droplets with varying cyclin B mRNA concentrations. Right: fluorescent profiles of two example droplets with different cyclin B mRNA concentrations, indicated by dashed lines in the left figure. (E) The rising and falling periods vs cyclin B mRNA concentration. Definitions of the rising and falling phases of the fluorescent profile are indicated in Figure 1B. Only the first cycle periods are included in the figure for clarity. (F) Relative period (normalized to maximum) when tuning cyclin B synthesis rate (minimum value to maximum is normalized to 0−1) in three models. Ksynth in Yang−Ferrell model[11] and k1 in Novak−Tyson-2equ[10] and full model[9] are perturbed to simulate mRNA variation. The initial parameter value is circled.

contributes to cell cycle oscillation and its dynamical properties.

2. RESULTS AND DISCUSSION

2.1. High-Throughput Microfluidic Platform to Study *Xenopus* Embryonic Cell Cycle. Previously, we have studied the cell cycle regulation of *Xenopus* egg extracts in droplets of varying sizes, ranging from 10 to 300 μm in diameter, created through vortexing.[17,18] The vortexing method enables high-throughput imaging of cell cycle progression in individual droplets across diverse droplet sizes in a single batch. However, postprocessing is needed to filter droplets of similar sizes, since we observed the cell cycle period is droplet size-dependent. Also, in order to quantitatively manipulate the composition of the droplets, such as varying the concentration or activity of cell cycle regulators, multiple batches need to be prepared manually.

To create droplets of uniform and programmable sizes, we used a single-channel microfluidic device to encapsulate extracts of certain constitutions and developed an automatic image processing method for single-cell segmentation and tracking.[19] To report cell-cycle dynamics, we supplemented the extracts with mRNA encoding for the chimeric fluorescent protein securin-CFP. The securin protein, a substrate of APC/C, is steadily accumulated throughout interphase due to synthesis from the securin mRNA, and sharply drops upon the onset of anaphase when the protein is ubiquitinated by the activated APC/C and targeted for degradation (Figure 1A). Each droplet showed an oscillating securin-CFP signal, indicating a successful constitution of cell cycle activities (Movie S1). Figure 1B shows an example trace of the securin reporter in a single droplet, with self-sustained oscillation signal of CFP throughout the timecourse. The number of cycles that each droplet sustains can vary from a few to over 20 cycles.

2.2. Single-Inlet Microfluidics to Create Uniform Droplets for the Estimation of System Variation. We first estimated the innate variations of our experimental platforms by using a single-inlet microfluidic device that generates droplets of cycling *Xenopus* egg extracts at a uniform size and constitution. Analysis of the temporal signal of securin-CFP oscillation revealed that initially the droplets were highly synchronized in the first few cell cycles (cycles #1−#4), but gradually desynchronized in later cycles (starting cycle #5) (Figure 1C,D; Movie S1). To identify the source of cell cycle desynchronization, we analyzed the variations (standard deviation or SD, and variance) of the droplet securin-CFP peak time (T_peak) of each cycle, from the 1st to the 15th cycle (Figure 1D), and observed a linear increase in the SD of the T_peak over the average time of the T_peak (Figure 1E, blue).

https://doi.org/10.1021/acssynbio.3c00631
ACS Synth. Biol. 2024, 13, 804−815

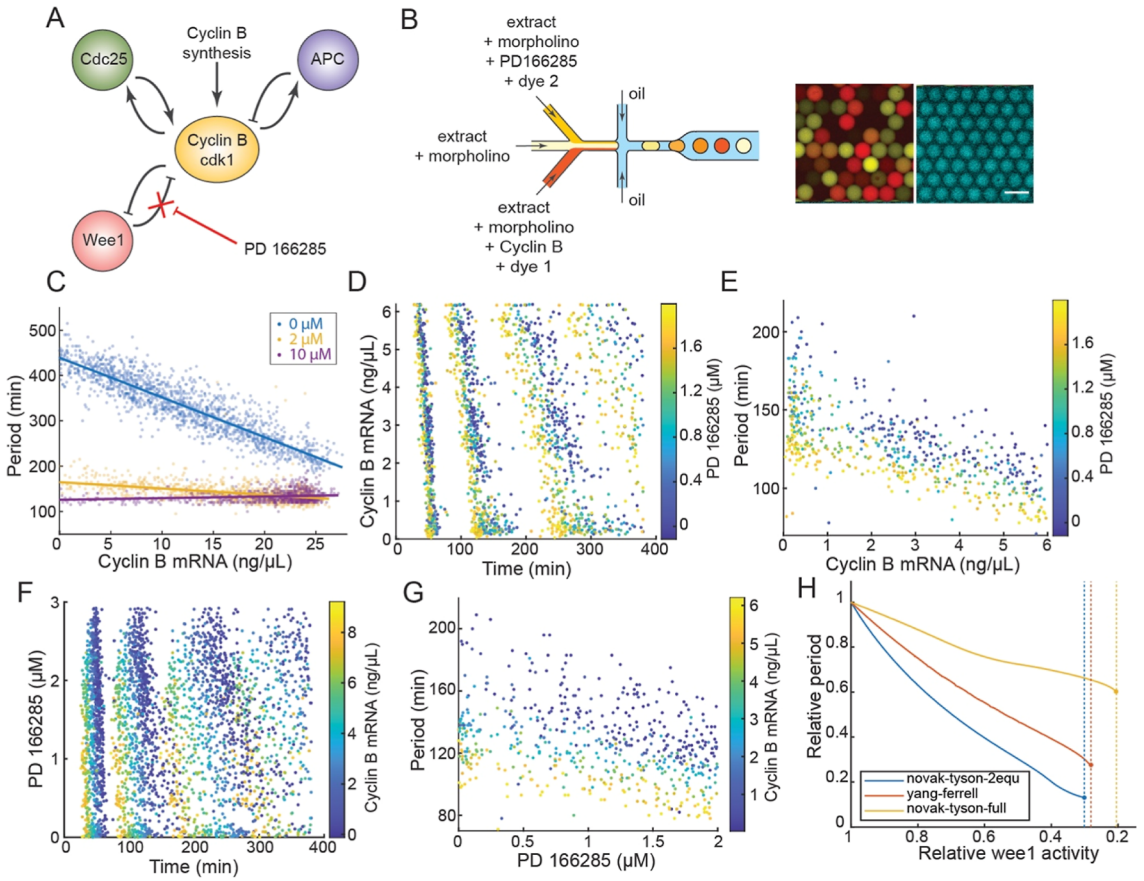

Figure 3. Inhibiting Wee1 positive feedback reduces period tunability. (A) Schematic view of the function of PD166285 on the mitotic circuit. (B) Left: schematic view of a three-channel microfluidic device. Fluorescent dyes are coadded with cyclin B mRNA and PD166285, respectively, to index their concentrations. Right: fluorescent images of droplets: composite of fluorescent dyes (left) and securin-CFP (right). Scale bar = 100 μm. (C) Period tuning by cyclin B mRNA under coarse-grained Wee1 perturbations. The colored scatter plots represent three distinct PD166285 concentrations. The lines indicate linear approximations of the experimental data. (D) Raster plot of droplets with varying cyclin B mRNA concentrations. (E) Scatter of the oscillation period vs cyclin B mRNA concentration. Only the first cycle periods are shown in the figure to eliminate the period elongation effect. (F) Raster plot of droplets with varying PD166285 concentrations. (G) Scatter of oscillation period vs PD166285 concentration. Only the first cycle periods are shown in the figure. (H) Relative period (normalized to maximum) when Wee1 activity is decreased in three different models. Decreasing of bwee1 in Yang−Ferrell model, kwee1 in Novak−Tyson-2equ and kwee1 in Novak−Tyson-full model is used to simulate the wee1 inhibitor effect. Dashed line indicates the relative wee1 activity level when oscillation is arrested.

If random phase diffusion dominates the system noise, the peak time variance should be linearly correlated with time.[20] Instead, our results showed a convex curve of peak time variance over time (Figure 1E, red). These results may be explained by the observation that the droplets generated from the same batch and constitution of extract had innate differences in oscillation periods, which becomes apparent when sorting all droplets by their average period (Figure 1D). A possible cause of the droplet period difference is the partitioning noise during the microemulsion encapsulation process.[21] Together, these results suggested that the major source of system noise is not the phase fluctuation of cell cycles but the initial period variation among the population of individual droplets that can propagate throughout cycles. Nevertheless, the droplet period noise (SD) is ∼8% of the average droplet period, which is still much lower compared with the effect of the perturbations used in the study (see sections below).

In addition, we found that the droplet oscillations gradually slowed down after the first three to four cycles with increasing periods (Figure 1B−D; Figure S1A,G,H). This is possibly caused by the depletion of some rate-limiting factors in the droplets, such as energy[17] or cyclin B1 mRNA. The first three cycles maintained a roughly constant cycle period, which is likely a more accurate representation of the physiological state of droplets. Therefore, in the following analyses of this study, we focused on only the first three cycles.

2.3. Development of a Multi-Inlet Microfluidic Platform for Comprehensive Parameter Space Perturbations. The single-inlet microfluidic device could generate only droplets with identical initial states, despite small variations, as described above. To enable global exploration in the parameter space, we extended our microfluidic design to incorporate up to three inlets prior to droplet formation. In this study, one of the inlets was reserved for unmodified *Xenopus* egg extracts, while the remaining channels were utilized to introduce recombinant mRNA molecules or chemical agonists/antagonists of cell cycle regulators for perturbation purposes. Content from the channels is mixed during droplet formation. The ratio of the content from the inlets can be dynamically adjusted by changing the pressure profile of the channels. The total sum of the flow rates from all channels is kept constant to ensure a constant droplet size. In this study, the droplet diameter is kept

https://doi.org/10.1021/acssynbio.3c00631
ACS Synth. Biol. 2024, 13, 804−815

at around 100 μm, which is comparable to early embryonic cells.

Consequently, depending on which of the single-inlet, two-inlet, or three-inlet microfluidic devices are employed, for any single batch of extracts, our microfluidic platform can be programmed to generate droplets of uniform size and multiple preset constitutions, such as discrete levels of a cell cycle regulator (Figure 1B), a continuous parametric sweep of one component (Figure 2A), or a two-dimensional array of two components (Figure 3B). Stable chemical fluorophores, such as Alexa 594 and Oregon Green, were used as indexing dyes for different inlets, so the composition of individual droplets can be quantified based on the fluorescent levels of these indexing dyes.

We used the anaphase substrate securin-CFP as a cell cycle reporter to monitor the cell cycle progression in all experiments of this study. To maintain a consistent concentration of the securin reporter mRNA in all droplets generated in a batch, we added mRNA to all inlets at the same concentration. We developed an in-house image processing and droplet tracking algorithm to track and quantify the securin-CFP dynamics in individual droplets.

2.4. Interphase Period Is Highly Tunable by Cyclin B Levels. Varying cyclin B synthesis rate could effectively tune the cell cycle duration, as previously demonstrated in both theoretical simulations[12] and experiments.[22,23] In our investigation, we aimed to generate an experimental data set to measure the cell-cycle response through a single−variable parameter sweep focusing on the cyclin B synthesis rate in both directions.

To tune down the cyclin B production rate in droplets, we designed and applied cyclin B morpholino antisense oligonucleotides to block the transcription of endogenous *Xenopus* cyclin B (x-cyclin B) mRNA species. A mixture of four morpholinos was used, two for cyclin B1 and two for cyclin B2 (Materials and Methods). We used a two-inlet microfluidic device, with one inlet injected with unmodified cycling *Xenopus* extract, and the other with extract containing additional morpholino mixture and an indexing dye (Figures 2A and S1B). By varying the pressure of the two inlets following a preprogrammed profile (Figure S1C), we generated droplets with a continuous gradient of morpholino concentration, ranging from 0 to 5 μM total morpholinos. For each droplet, the concentration of added morpholinos was calibrated by the fluorescence intensity of the indexing dye (Figure S1D).

Morpholino addition significantly slowed endogenous oscillations with up to 5-fold increase in the cell cycle period (Figure 2B,C), affirming that the cyclin B level significantly affects the cell cycle period. However, not all phases of the cell cycle are equally affected. The rising phase of the securin-CFP oscillation, which comprises mainly the interphase and the initial part of the M-phase, showed a roughly linear increase in duration, whereas the falling phase, approximately corresponding to the start of the anaphase until mitotic exit, maintained a relatively constant duration (Figure 2C). The insensitivity of the falling phase period to cyclin B variation is consistent with previous reports that the mitotic phase is temporally more robust compared to other phases, which can be explained by the positive feedback loops in the mitotic circuit.[19,24]

We then examined cell cycle dynamics when introducing additional recombinant human cyclin B (h-cyclin B) mRNAs to the extracts that were treated with 5 μM morpholinos to deplete endogenous cyclin B mRNA. We used the same two-inlet microfluidic device to generate droplets having 0 to 25 ng/μL h-cyclin B mRNAs. In the absence of h-cyclin B mRNA, the system oscillated at a speed similar to that observed when 5 μM morpholino was applied, likely driven by residual endogenous x-cyclin B mRNA. The addition of h-cyclin B mRNA significantly accelerated cell cycle oscillations with up to a 4-fold increase in the cell cycle frequency. Consistent with the impact of morpholinos, only the period of the rising phase significantly shortened with increasing cyclin B mRNA concentration, whereas the falling phase period was almost unaffected (Figure 2D,E). Both the cyclin B mRNA and morpholino tuning consistently demonstrated that the cell cycle period monotonically and gradually decreases with an increasing cyclin B synthesis rate.

With these data sets, we could evaluate the three published cell cycle models to test if they correctly recapitulate the cell cycle response to cyclin B tuning. All three models assumed that the oscillation is driven by the negative feedback loop between cyclin B-Cdk1 and APC/C, but they used different rate equations. The Yang−Ferrell model[11] and Novak−Tyson-2equ model[10] are simple two-equation systems that use Hill function and Goldbeter−Koshland kinetics,[25] respectively, to construct the rate equations. The third, Novak−Tyson-full model is a detailed mass action model with 10 equations.[9] All three models correctly predicted the cell cycle responses to mRNA concentration at a relatively low cyclin B synthesis rate (Figure 2F). However, at a high cyclin B synthesis rate, both Yang−Ferrell's two-equation model and Novak−Tyson's full model showed a slight increase in the oscillation period, which was not experimentally observed. The increase in period at high cyclin B levels in the two models resulted from the increases in the period of falling phase of cyclin B (i.e., late mitotic phase) (Figure S2H), presumably because faster synthesis rate resulted in more cyclin B proteins being degraded at the falling phase. In contrast, Novak−Tyson's two-equation model recapitulated the monotonic and gradual decrease of cell cycle period with increasing cyclin B synthesis rate, presumably because the Michaelis−Menten kinetics derived steady state allowed a faster initial degradation of cyclin B protein. The Novak−Tyson-2equ model is the only one of the three models tested that uses Goldbeter−Koshland kinetics, which fits experimental observations better than the other two models; thus, these results suggest that the dynamics of Wee1−Cdk1 and Cdc25−Cdk1 regulations under fast equilibrium assumption, used in both the two-equation models, might be better modeled by Goldbeter−Koshland kinetics.

2.5. Wee1 and Cdc25 Positive Feedback Loops Increase Cell Cycle Period Tunability. Theoretical studies have suggested that the strength of the Cdk1/Cdc25/Wee1 positive feedback is essential for the period tunability by cyclin B.[12] To examine such a relation, we applied a three-inlet microfluidic platform to simultaneously vary the positive feedback strength and the cell cycle speed by changing the cyclin B synthesis rate (Figure 3). This systematic mapping of the cell cycle period landscape can inform how the period tunability responds to fine-tuning of the feedback strength.

To suppress the positive feedback strength, we compromised the kinase activity of Wee1 with chemical tyrosine kinase inhibitor PD166285[26] (Figures 3A and S2A−C). Note that applying a Wee1 inhibitor also inevitably suppresses the Cdc25 positive feedback loop because Wee1 and Cdc25 antagonistically regulate the same phosphate groups of Tyr15 and Thr14

https://doi.org/10.1021/acssynbio.3c00631
ACS Synth. Biol. 2024, 13, 804−815

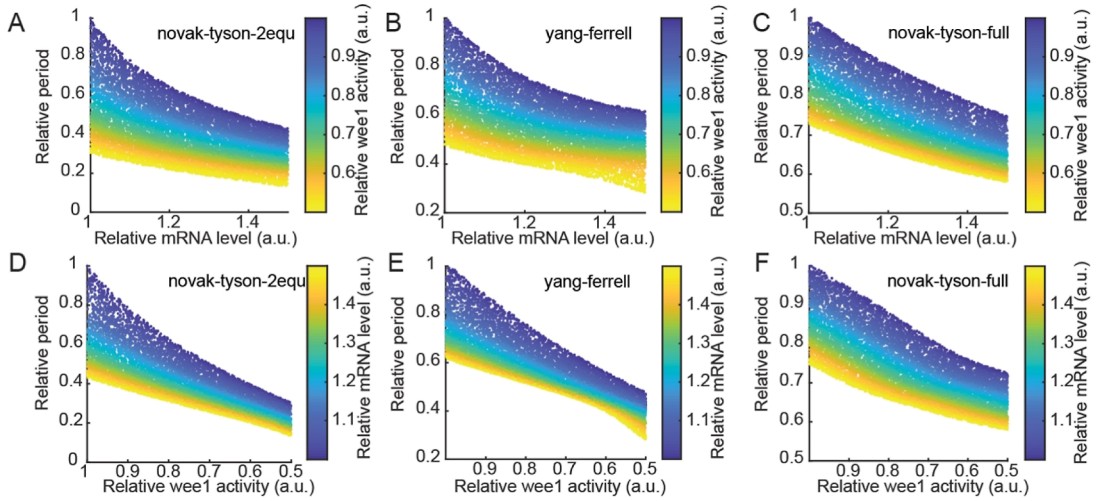

Figure 4. Computational simulation of cell cycle frequency change by perturbing cyclin B or Wee1 activity. (A−C) Period response of relative cyclin B mRNA activity in Yang−Ferrell model,[11] Novak−Tyson-2equ[10] and Novak−Tyson-full[9] model, respectively, color code Wee1 activity. (D−F) Period response of Wee1 activity inhibition Yang−Ferrell model, Novak−Tyson-2equ and Novak−Tyson-full model, respectively, color code mRNA concentration.

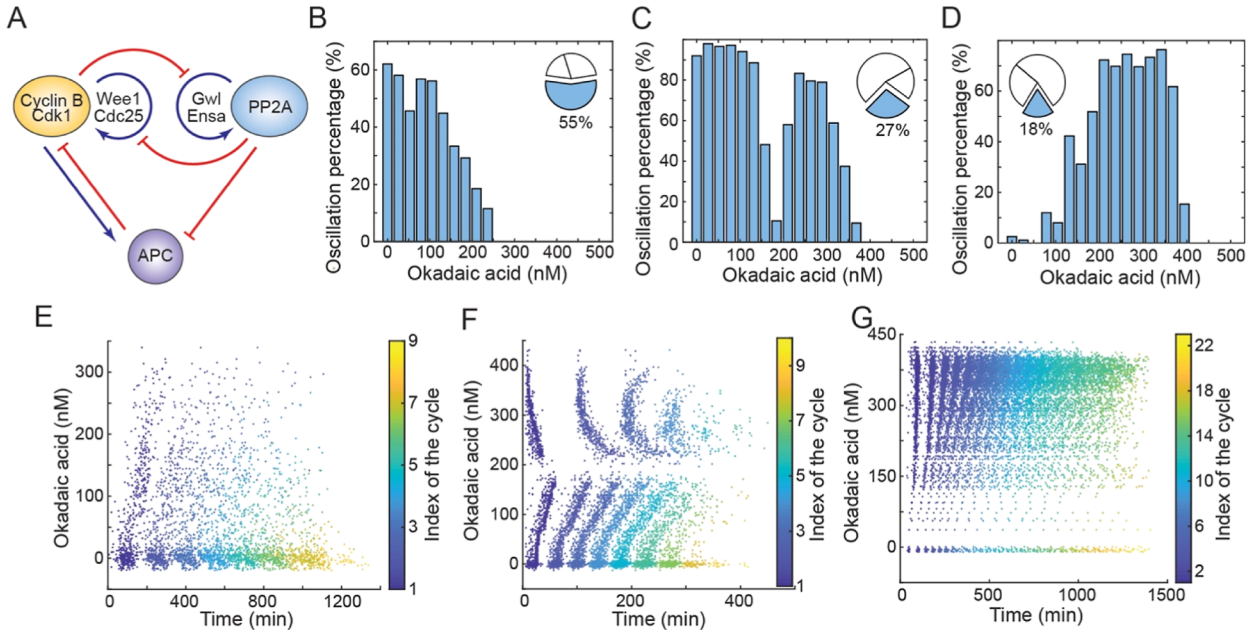

Figure 5. Inhibiting PP2A leads to multimodal responses in the oscillation and period. (A) Schematic view of molecular circuits including PP2A activities. (B−D) Percentage of oscillatory droplets vs OA concentration, showing type 1 (B), type 2 (C), and type 3 (D) responses. Pie chart shows the percentage of each response type observed in all experiment results. (E−G) Representative raster plots of type 1 (E), 2 (F), and 3 (G) responses to OA concentration. Droplets are sorted by OA concentration, and the color codes for the index of the cycle, or the cycle number.

on Cdk1. We first applied different concentrations of PD166285 and performed two-channel cyclin B mRNA tuning to test if the cell cycle period tunability is affected. The results revealed that while droplets with no PD166285 showed a wide range of oscillation frequencies, this range was dramatically reduced when 2 μM or more of the inhibitor was present (Figures 3C and S2D). In the group with the highest inhibitor concentration (10 μM), the extent of period change was similar to the background noise level. This suggested that interrupting Cdc25/Wee1-based positive feedback could impose a significant impact on the cell cycle tunability, even though the cell cycle oscillations were sustained.

We then used the three-inlet setup to generate a fine-grained tuning of both cyclin B concentration (by adding 0 to 6 ng/mL h-cyclin B mRNA to extracts supplied with 5 μM x-cyclin B morpholinos) and Wee1 activity (by 0 to 2 μM PD166285) (Figures 3B and S2E). We programmed a three-inlet pressure profile (Figure S2F), so that the generated droplets have relatively uniform distributions of PD166285 and cyclin B mRNA concentrations (Figure S2G; Movie S2). The results showed that increases in the PD166285 concentration gradually reduced the range of droplet cell cycle periods under the same tuning range of cyclin B mRNA concentration, and the difference is more evident in the lower cyclin B mRNA concentration region (Figure 3D−G).

To examine if computational models could recapitulate the observed results, we then perturbed parameters representing the Wee1 activity in the aforementioned three models. We first

https://doi.org/10.1021/acssynbio.3c00631
ACS Synth. Biol. 2024, 13, 804−815

examined the model responses to Wee1 without cyclin B tuning. When decreasing Wee1 activities to 20−30%, all models showed an oscillation arrest (Figure 3H), which was not observed experimentally at 10 μM PD166285 (Figure 3C). This suggests that these three models were incomplete and other components may be required to properly explain the cell cycle dynamics when Wee1 is inhibited.

We next examined model responses to Wee1 under cyclin B tuning to test how Wee1 activity and its associated positive feedback loops affect the cell cycle period tunability. We simulated each of the three models and calculated the period range as we tuned both cyclin B synthesis rate (Figure 4A−C) and Wee1 activity (Figure 4D−F), respectively. All three models captured the overall trend and range of cycle periods in response to changes in both cyclin B mRNA levels (Figure 3E vs Figure 4A−C) and Wee1 activity (Figure 3G vs Figure 4D−F). In general, the Novak−Tyson-2equ model seems to best describe the experimental behavior; the Yang−Ferrell model showed unexpected frequency tunability increases in high mRNA and high Wee1 domains, while the Novak−Tyson-full model showed smaller tunability decrease compared with experimental results. These results indicate that the existing models could predict the local response to changes in Wee1 activity and cyclin B mRNA levels but failed to recapitulate experimental results in high Wee1 inhibitor concentrations, suggesting the possible contribution of other mechanisms in addition to the Cdk1/Cdc25/Wee1 positive feedback.

2.6. PP2A Is Required for Cell Cycle Oscillation. Other than the extensively characterized Cdk1/Cdc25/Wee1 positive feedback, studies have identified additional positive feedback regulation centered on the Cdk1-counteracting phosphatase, PP2A[14] (Figures 5A and S5E). PP2A dephosphorylates many Cdk1 substrates, including Wee1, APC/C, and Cdc25.[27] In addition, PP2A forms a double negative feedback loop with the Endosulfine Alpha/Greatwall (ENSA/Gwl) pathway. Recent studies[15,16] reported that the PP2A-ENSA/Gwl feedback loop is necessary for the bistability of Cdk1 substrate phosphorylation. However, it is unclear whether PP2A affects cell cycle dynamics.

To study the influence of PP2A on the cell cycle, we applied okadaic acid (OA), a PP2A inhibitor with a reported IC_{50} of 0.14 nM in vitro[28] to tune PP2A activity in our droplet cells. Using two-channel tuning, we generated droplets of OA concentration ranging from 0 to 600 nM. We observed that PP2A inhibition by OA had a significant impact on cell cycle dynamics, and droplets treated with >500 nM OA had always shown a complete cell cycle arrest (Figure 5B−G; Figure S5A−C). These results supported that unlike Wee1, which could be fully inhibited without terminating cell cycles, PP2A activity is necessary for mitotic oscillation.

2.7. Cell Cycle Dynamics Exhibits Multimodal Responses to PP2A Inhibition. Furthermore, we observed that cells responded to OA inhibition in distinct patterns that appeared to be batch-dependent. Across 11 independent experiments with identical setups, we observed three distinct types of response patterns. The first type, observed in over half (6 times) of the experiments, was characterized by a gradual decrease in the percent of oscillating droplets as OA concentration increased from 0 to 300 nM and a complete cell cycle arrest at higher OA levels (Figure 5B,E; Figure S5A). The second type, which was less frequent (appeared three times), showed a similar response as in type 1 in the lower OA region, but at higher OA, droplets "resumed" robust oscillation (Figure 5C,F; Figure S5B). In other words, the type 2 response was characterized by a gap at an intermediate OA level, where the cell cycle was arrested. For the third, the least frequent type (appeared twice), only a small percent of droplets had oscillations at low OA, but as OA increased, droplets showed an increasing tendency to oscillate before the percent of oscillating droplets dropped again as OA reached 400 nM (Figures 5D,G and S5C). Therefore, the type 3 response resembled the trend seen in the second half of the type 2 response (after the gap).

We next examined the effects of PP2A inhibition on the cell cycle period and also observed responses of multiple forms (Figure S5G−I). Because of the infrequent occurrences of type 2 and type 3 responses, we focused on period analysis for type 1 only. The cell cycle period showed either a monotonic decrease (Figure S5G), a monotonic increase (Figure S5I), or a slight decrease followed by an increase (Figure S5H). We then separately examined the durations of the increasing phase (i.e., interphase and early mitotic phase) and decreasing phase (corresponding to the late mitotic phase after the anaphase substrates, cyclin B or securin proteins, started to decay) (Figure 7A,C,E). This revealed that the multimodal responses in the cell cycle period mainly reflected the multimodal changes in the increasing phase. In contrast, the duration of the decreasing phase remained a simple increasing trend in all tested conditions, although the slope of the increases varied.

These different responses were not caused by technical errors, such as uneven sampling of OA concentrations in the droplets, as checked by sampling histograms (Figure S5A−C). To further confirm the observations were independent of channel-tuning setup, especially to verify the rare type 2 bimodal distribution that was never reported before in literature, we performed alternative experiments using coarse-grained manual tuning. We divided the same batch of extract into separate tubes each treated with OA at a final concentration of 0, 50, 100, 200, 400, and 800 nM. We then used single-inlet microfluidics to create identical droplets for each OA group. One of the experiments clearly recapitulated the type 2 response: oscillations were self-sustained at 0, 50, and 400 nM but arrested at 100, 200, and 800 nM (Figure S5D; Movie S3). These experiments ruled out potential technical artifacts associated with the multi-inlet sampling, suggesting that the multimodal phenomena observed could reflect biological heterogeneity of the system.

We also checked to rule out any drug-specific artifacts, e.g., off-target effects of OA. Despite its prevalent usage as a PP2A inhibitor, OA can also inhibit PP1 when applied at high concentrations (IC_{50}—300 nM in vitro[28]). We therefore tested additional PP2A inhibitors, endothall and fostriecin, which are less effective at inhibiting PP1, as well as IPP2 (protein phosphatase inhibitor 2), a predominant PP1 inhibitor (Materials and Methods). We found that these alternative PP2A inhibitors showed a similar response as OA, whereas PP1 inhibitors had different effects on the droplet mitotic cycle (Figures S3 and S4). Moreover, droplets prepared from the same *Xenopus* extract batch but treated with different PP2A inhibitors showed the same type of responses. These results suggested that the multimodal responses were specific to PP2A inhibition and were extract batch-dependent.

Altogether, these results suggest that PP2A activity can significantly affect the cell cycle dynamics. At high inhibitor concentrations, when PP2A is mostly inhibited, the cell cycle is fully arrested. However, partial inhibition of PP2A may pose

https://doi.org/10.1021/acssynbio.3c00631
ACS Synth. Biol. 2024, 13, 804−815

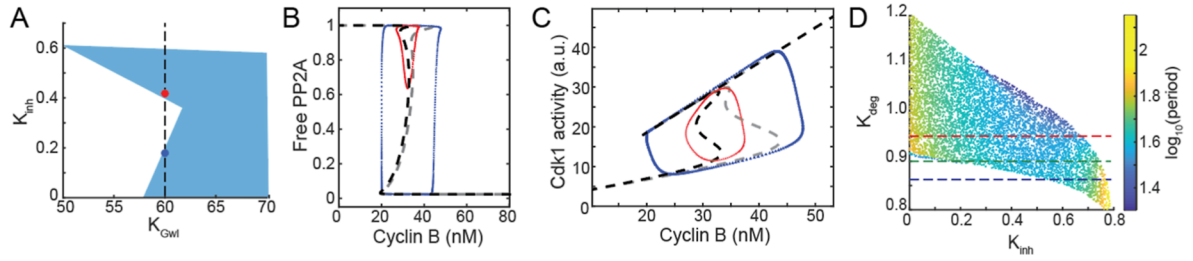

Figure 6. Mathematical model and numerical simulation of PP2A inhibition on cell cycle oscillation. (A) Parameter regions that support oscillation when changing K_{gwl} and K_{inh} (OA). Changing K_{inh} at a specific value of K_{gwl} (along the dotted black line) may lead to a type 2 OA response. Blue and red dots show oscillations in low and high OA concentration, respectively. (B,C) Dashed lines show response curves of steady-state free PP2A (B) or Cdk1 (C) activity when changing cyclin B concentration under low (gray) or high OA (black). Dotted lines show phase plots of limit cycles with low (blue) or high (red) OA corresponding to (A). (D) Oscillation period (color-coded) changes when tuning K_{inh} (OA concentration) and relative EC_{50apc} (activity threshold for the Cdk1 substrate). Red, green, and blue dotted lines show three different OA period responses.

different effects on the cell cycle oscillator. The fact that the droplet response depends on the batches of extracts but not the types of PP2A inhibitors strongly suggests that the distinct response patterns arise from variations in the endogenous properties of the *Xenopus* extract batches. Possible sources of such variations include biological heterogeneity in frogs and the maternally deposited materials in batches of *Xenopus* eggs as well as uncontrollable day-to-day variability in the extraction preparation processes. Modeling could help understand the underlying circuit design that makes the system's response to PP2A sensitive to these variations.

2.8. Modeling Suggests That Greatwall Variations Can Result in the Multimodal Responses of Cell Cycle Dynamics to PP2A Inhibition. To understand why the partial inhibition of PP2A resulted in qualitatively different responses, we applied mathematical modeling and computational simulation. Because there has not been a well-recognized model that describes embryonic cell cycle oscillation of *Xenopus* extract that considers PP2A/Gwl/Ensa, and the existing model we tested could not recapitulate experimental perturbation in our system (Figure S5J−L), we developed a new model based on the Yang−Ferrell model and the PP2A−Cdk1 interactions proposed in Kamenz et al.[16] (Figures 5A and S5E). This simple model contains four variables (including concentrations of activated Cdk1, cyclin B, free PP2A, and phosphorylated Ensa) and 26 parameters. We verified that this new model could perform as well as the other three models in terms of recapitulating the mRNA and Wee1 perturbation results (Figure S2I−K). To examine the mechanism of multimodal response, we hypothesized that batch-to-batch variations in the concentration of certain molecules and/or their chemical properties in the *Xenopus* extract resulted in a differential response of the mitotic oscillator to PP2A partial inhibition. Therefore, we applied random sampling in the 22-dimension space of model parameters that reflect extract properties, excluding four parameters representing Hill coefficients that are unlikely to vary in different extract batches. We therefore searched for the parameter that has the highest association to causing multimodal responses with increasing PP2A inhibitor level (modeled as an additional parameter K_{inh}).

To reduce the computational load, we first searched ∼50,000 random parameter sets for model perturbations that can result in the characteristic type 2 response, which involves a gap of arrested cell cycle oscillation at intermediate concentration of PP2A inhibitor, while oscillations persist at both sides of the gap, and a full oscillation arrest at high PP2A inhibition, namely, an oscillate-arrest-oscillate-arrest behavior. This revealed that only a rare fraction (15 points, ∼0.3%) of the conditions exhibited this behavior.

Next, we examined these conditions and the distributions for each of the 22 perturbed parameters. Interestingly, although most parameters followed a relatively uniform distribution covering a wide sampled range, one parameter, K_{gwl} (EC_{50} of Cdk1 phosphorylating Gwl), showed a narrowed distribution (Figure S5M). This suggested that a type 2 response requires a specific value range of the K_{gwl}. Consequently, we tested if changing K_{gwl} would result in type 1 and 3 responses of the model while maintaining other parameters at the centroid of the previously identified points that support type 2 responses. Indeed, we found that higher K_{gwl} resulted in type 1 response, whereas lower K_{gwl} resulted in a type 3 response (Figure 6A). This finding suggested that the frog extract variations in Greatwall could explain the puzzling multimodal responses of cell cycle oscillation to PP2A inhibition. In support of the model prediction, Kamenz et al. measured K_{gwl}, and found about an approximately 2-fold variation in its level among three replicate experiments.[16]

To understand how changes in K_{gwl} lead to different responses in the oscillator, we plotted the steady state response curves of free PP2A to cyclin B (Figure 6B), active Cdk1 to cyclin B (Figure 6C), and PP2A to Cdk1 (Figure S5F), respectively. This revealed that our cell cycle model can switch between two different stable limit cycles under partial PP2A inhibition. Previous theoretical studies reported the existence of diverging oscillators, which exhibit sharp period changes near saddle-node on invariant circle (SNIC) bifurcation points.[29] To explore the mechanism of the switch, we performed bifurcation analysis with changing OA concentration (K_{inh}) (Figure S6E,F). The results show that as K_{inh} increases, the solution of the system changes from one limit cycle (Figure S6A), to one steady state (Figure S6B), to one limit cycle and one steady state (Figure S6C), and to two steady states (Figure S6D). We also simulated the period (Figure S6G) and PP2A amplitude (Figure S6H) of the limit cycles. We found that the first limit cycle (low OA) disappears with a changing period and stable amplitude, suggesting saddle-node bifurcation, while the second limit cycle (high OA) collapses through Hopf bifurcation with a changing amplitude and stable period. Intuitively, when the OA level is low, the cell cycle oscillates between high and low steady states of PP2A, resulting in a high-amplitude cycle (blue limit cycle in Figure 6B,C). Cell cycles from the type 1 response and the type 2 first-half response (before the gap) belong to this type

https://doi.org/10.1021/acssynbio.3c00631
ACS Synth. Biol. 2024, 13, 804−815

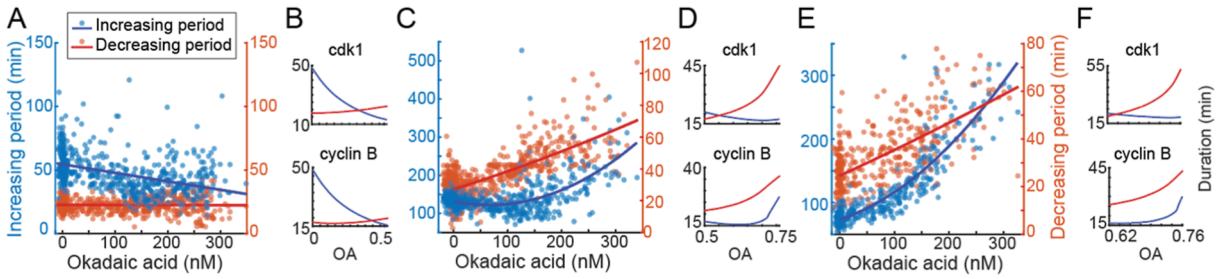

Figure 7. Dynamics of different phases of the cell cycle in response to PP2A inhibition. (A,C,E) Experimental results of increasing and decreasing period when tuning OA, showing three different types of period response: monotonically decreasing (A), decreasing and then increasing (C), or monotonically increasing (E). Solid lines are fitted curves with linear or quadratic regression. (B,D,F) Simulated results of increasing and decreasing period of cyclin B concentration and Cdk1 activity when adding OA, corresponding to three different types of responses. The simulated period changes in cyclin B shared similar trends with securin measured in (A,C,E), while trends in Cdk1 activity were consistent across the three conditions.

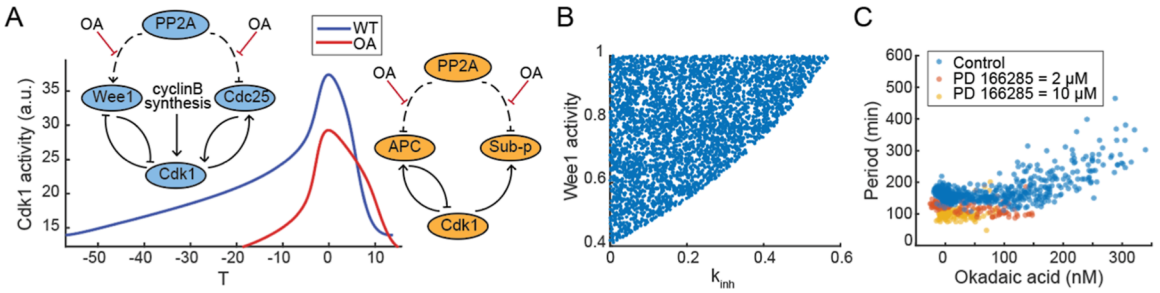

Figure 8. Changes in cell cycle oscillation in response to both Wee1 and PP2A inhibition. (A) Representative time series of Cdk1 activity of WT- and OA-treated cycles. The schematic molecular circuits show different OA effects during increasing and decreasing phases of oscillation. (B) Oscillatory region when tuning Wee1 activity and K_{inh} (OA) in a computational model showing that Wee1 inhibition leads to a smaller region of oscillation when adding OA. (C) Period responses to OA when PD166285 was added in different concentrations.

of oscillation. When the OA level is high, Wee1 and Cdc25 are hyperphosphorylated, causing easier Cdk1 activation. As a result, the peak Cdk1 activity is lower and could not fully inhibit PP2A to trigger PP2A-ENSA-Gwl bistability. The oscillation occurs between the intermediate and high steady states of PP2A (red limit cycle in Figure 6B,C). In this case, the oscillation is solely driven by bistability based on Wee1/Cdc25 positive feedback. Cell cycles from the type 3 response and the type 2 s half-response (after the gap) belong to this type of oscillation.

2.9. Modeling Suggests That APC/C Variations Can Result in Multimodal Responses in Cell Cycle Period to PP2A Partial Inhibition. Although variations in Gwl might account for polymodal patterns in cell cycle oscillations, they did not explain the variations in cell cycle period response when tuning PP2A, implying the potential involvement of other molecules. Because the negative feedback core of an oscillator (i.e., the Cdk1-APC/C negative feedback loop in the cell cycle) could significantly affect the oscillator period, we hypothesized that variations in relative APC/C activity (K_{deg}) could result in the variations in the cell cycle period response observed for type 1 responses. Using the same model, we varied K_{deg} and examined the changes in period while varying PP2A inhibition (K_{inh}). As hypothesized, we found that small variations in K_{deg} can result in different period responses (Figure 6D). Specifically, the oscillating period monotonically decreased over K_{inh} at high K_{deg}, monotonically increased at low K_{deg}, and showed a decrease-then-increase trend at intermediate K_{deg}.

To gain further insights into the cell cycle period variations over OA, we divided the cell cycle into increasing and decreasing phases (Figure 7A,C,E), following the previous definitions in experimental analyses (Figure 2C,E). Experimentally, we used securin-CFP as our cell cycle reporter, which is not a model variable. However, both securin and cyclin B are substrates of APC/C, accumulating via protein translation in the interphase and degrading at the onset of anaphase; therefore, the two proteins should share similar increasing and decreasing phases. Indeed, we found that the trend for cyclin B increasing and decreasing phases in the model resembles that of the securin-CFP in the experiments (Figure 7B,D,F, lower panel). We also examined the changes in the duration of increasing and decreasing phases of Cdk1 activity when tuning PP2A (Figure 7B,D,F, upper panel). Interestingly, the Cdk1 increasing and decreasing phase durations were conserved across all conditions: the Cdk1 increasing period had always decreased with OA concentration, whereas the decreasing period increased. This result suggests that the variations in period response are determined by the relative sensitivity of the increasing/decreasing phase of Cdk1 activity to PP2A inhibition. As illustrated in Figure 8A, PP2A inhibition affects both the mitotic entry and exit. During mitotic entry, PP2A inhibition inhibits Wee1 but activates Cdc25, which reduces the threshold of Cdk1 activation and leads to an accelerated cell cycle progression. However, during mitotic exit, applying the PP2A inhibitor complicates the ability of APC/C to deactivate and leave mitosis, which prolongs the mitotic phase, and at high concentration, it leads to cell cycle arrest.

2.10. Changes in Cell Cycle Oscillation in Response to Both Wee1 and PP2A Inhibition. To understand how the Cdk1/Cdc25/Wee1 and PP2A/ENSA/Gwl positive feedback

https://doi.org/10.1021/acssynbio.3c00631
ACS Synth. Biol. 2024, 13, 804−815

loops work together to influence cell cycle period tunability, we simulated the PP2A cell cycle model in response to changes in both Wee1 and PP2A levels (Figure 8B). Interestingly, we found that inhibitions of PP2A (K_{inh}) and Wee1 reduced each other's range to sustain oscillations. To test this observation, we used the two-inlet system to generate droplets of *Xenopus*extract and tuned the concentration of OA under three different levels of Wee1 inhibitor PD166285. In support of the model prediction, higher PD166285 indeed reduced the OA tuning range that supports oscillation and the range of oscillation periods (Figure 8C).

3. CONCLUSIONS

While mathematical models have often been built to understand biological systems under specific conditions, their effectiveness is difficult to evaluate across perturbed environments. In our study, we have developed a platform to systematically perturb system parameters and utilized it to challenge existing cell cycle models. We found that most cell cycle models could predict the system's response to cyclin B mRNA tuning, but not global Wee1 or PP2A perturbations. By combining and modifying existing models, we constructed a new model that could predict all of the perturbation effects in our study. This approach could help us to understand the limitations of current models and identify biological mechanisms that contradict models derived from past hypotheses.

Through global parameter searching, we also made new discoveries for comprehensive understanding of positive feedback regulations on cell cycle dynamics, which would be challenging to recapitulate through low-throughput studies of a few specific phenotypes. Many biological oscillators have well-conserved positive feedback despite the fact that, in theory, single time-delayed negative feedback is sufficient to generate sustained oscillations. Although extensive computational work has been done, suggesting that positive feedback may play a role in clock tunability and robustness, essential experimental studies in this regard have been missing. With our platform, we analyzed the whole spectrum of phenotypes by high-resolution mapping of the period landscape over perturbations in multiple dimensions, which provides comprehensive information necessary for testing theories and understanding the underlying mechanisms at the systems level. We showed that the previously proposed Cdk1/Cdc25/Wee1 positive feedback only contributes partially to the tunability of the cell cycle, and Wee1 inhibition alone could not abolish oscillations. These results inspired us to dissect the role of the additional positive feedback involving PP2A. Intriguingly, we observed multimodal behaviors in both oscillatory percentage and period. While we have not yet fully understood the mechanisms underlying these phenomena, our model suggests that the multimodal behaviors could be explained by the relative sensitivity of Cdk1's substrate Gwl or APC/C to Cdk1. The sensitivity of a substrate can be considered in terms of how soon the substrate is activated in response to Cdk1 activation. This highlights the importance of the temporal order of activation of APC/C and Gwl, and a slight change in the temporal order of the cell cycle may result in substantial changes in oscillatory patterns.

While future studies are required to verify these observations in live embryos, our findings in synthetic cells suggested that there could be more than one mode of cell cycle behaviors, and the oscillation properties and the temporal order of mitotic events might vary in these different oscillatory modes. These complex behaviors could not have been detected by conventional low-throughput and low-resolution network perturbations in live embryos or bulk extract assays. Our high-dimensional, high-throughput, high-resolution framework provides a generalizable strategy to explore frequency regulation in other biological oscillators, which may lead to a more comprehensive quantitative understanding of this fundamental phenomenon shared by biological clocks.

4. MATERIALS AND METHODS

4.1. *Xenopus* Cycling Extract Preparation. The preparation of cycling extract using *Xenopus laevis* eggs has been described in previous publications.[18] The frogs are primed with an injection of 100 IU human chorionic gonadotropin (HCG) 1 week before and again with 600 IU HCG 12−16 h before harvesting the eggs. The cytosolic materials were extracted via two-step centrifugation at 20,000*g*. Fluorescent dyes, cell cycle markers, and molecules of interest were then added directly to the extract and gently mixed before droplet generation.

4.2. Droplet Generation with Microfluidic Devices and Content Tuning. The method for microfluidic device fabrication, droplet generation, and loading was described in our previous report.[18] A multichannel pressure controller was used instead of a syringe pump to control the flow with precision. Cycling extracts with different molecules of interest were flowed in through different inlets before droplets were generated. The temporal pressure profiles of individual inlets were programmed to change periodically while keeping the combined aqueous pressure constant (Figures S1C and S2F), yielding droplets with different concentrations of these molecules in a wide yet continuous range. The concentrations of the molecules of interest were visualized by coadding fluorescent dyes of different colors to the extract and creating an index for every droplet, where the fluorescence intensity can be converted to actual concentration when calibrated with reference droplets.

4.3. Time-Lapse Image Acquisition and Image Analysis. The droplets were loaded into thin glass tubes precoated with trichloro(1*H*,1*H*,2*H*,2*H*-perfluorooctyl)silane to form a 2-D single droplet layer and then immersed in a glass-bottom Petri dish filled with mineral oil to prevent sample evaporation. The dish was then loaded into an inverted fluorescence microscope. Droplets were excited by a LED fluorescence light source, and images were then captured by a digital CMOS camera (exposure times: bright field, 1 ms; CFP, 400 ms; YFP, 200 ms; RFP, 200 ms). Automatic stage positioning and imaging were controlled by Micro-Manager, open-source microscopy software. The images were processed with a custom pipeline of MATLAB scripts. Individual droplets were segmented and tracked using bright-field images. Segmentation was achieved by a watershed algorithm with a seed generated from Hough circle detection. Tracking was performed by maximizing the segmentation feature correlation between two consecutive time frames. Fluorescent intensity profiles of the droplets were then extracted for further analysis. The oscillation period is defined by the time interval between two securin-CFP peaks. Intervals between two troughs behave similarly (Figure S1E). Oscillation amplitude is defined by the fluorescent intensity difference within a cycle. The intensity difference between each peak and previous trough is highly correlated with the intensity difference between each peak and following through (Figure S1F).

https://doi.org/10.1021/acssynbio.3c00631
ACS Synth. Biol. 2024, 13, 804−815

4.4. Numerical Simulation and Oscillator Detection. The numerical simulation is performed in Matlab using the ode15s function with a relative error of 10^{-6} and absolute error of 10^{-8}. Each system was simulated from $t = 0$ to $t = 5000$ (arbitrary unit). We applied the same method as published previously to detect limit cycle oscillations.[30] During simulation, if a system reaches steady state, then it is not an oscillator. At the same time, we monitored the recurrence of the states of the nodes. The peak of a specific node is selected as a reference. Let the time at peak i be t_i, and the values of all nodes are (x_i, y_i, z_i). If at least N consecutive ($N = 7$ in our simulation) peaks that satisfy $d(x_i,y_i,z_i),(x_{i+1},y_{i+1},z_{i+1}) < \varepsilon$ ($\varepsilon = 10^{-2}$) are found, and if the system satisfies: (1) stable amplitude: $\frac{\mathrm{std}(x_i)}{\mathrm{mean}(x_i)} < \sigma$, $\sigma = 10^{-2}$ and (2) stable period: $\mathrm{std}(t_{i+1} - t_i) < \delta$, $\delta = 10^{-2}$, then the system is considered an oscillator.

4.5. Statistical Analysis. In the context of our experiments, biological replication is defined as repeating one experiment of a certain setup design using different batches of *Xenopus* extracts, generating droplets with the same tuning parameters; technical replication is defined as one experiment using the same batch of *Xenopus* extracts, having multiple droplets with the same concentration of the molecules of interest (with random fluctuations considering that the concentration in each droplet is subject to partitioning error during the droplet generation process and covers a continuous range).

To ensure the experiment results are reliable and reproducible, every experiment has a minimum of three independent biological replicates. However, typically only one representative data set is presented in each figure mentioned above.

Data from individual droplets are selected for analysis only if: the droplet is in view the whole time during the time-lapse image acquisition and is tracked correctly from the beginning to the end. Any droplet that does not fit the criteria above is excluded from the analysis and figures.

In Figure 1C, $N = 79$ droplets are detected and are presented in the figure on the left. After discarding droplets that do not have complete traces mostly due to the movement of droplets in or out of view, $N = 64$ droplets are presented in 1D. Figure 1E uses the same data set as Figure 1D, each data point represents the average of $N = 64$ droplets, fitting of the data is achieved with the polyfit function in MatLab.

Figure 2B,C is plotted from the same data set with $N = 1021$ droplets, but Figure 2B shows all cycles, while Figure 2C only shows information from the second cycle. Figure 2D,E is plotted from the same data set with a sample size of $N = 974$ droplets, but Figure 2D shows all cycles, while Figure 2E only shows information from the second cycle.

Figure 3D−G is plotted from the same data set with $N = 704$ droplets. Figure 3E,G shows the third cycles selected from Figure 3D,F, respectively, with $N = 486$ droplets.

Figure 4 shows the results of 10k numerical simulations performed with MATLAB.

Figure 5B−D shows the percentage of droplets that can oscillate at different OA concentrations. All detected droplets, both oscillatory and nonoscillatory, are first binned according to OA concentration; then, the percentage of oscillating droplets is calculated for each bin. Figure 5B has a sample size of 1085 droplets, out of which 295 have oscillations displayed in the histogram; Figure 5C has a sample size of 1191 with 630 oscillating; and Figure 5D has a sample size of 885 with 482 oscillating.

In Figure 7A,C,E, $N = 576$, 603, and 371 droplets are presented, respectively. Linear fitting is used to represent the general trend in Figure 7A, and quadratic fitting is used in Figure 7C,E.

In Figure 8C, the sample size of each PD166285 concentration group is 0 μM, $N = 603$; 2 μM, $N = 113$; 10 μM, $N = 168$.

■ ASSOCIATED CONTENT

Supporting Information

The Supporting Information is available free of charge at https://pubs.acs.org/doi/10.1021/acssynbio.3c00631.

Additional materials and methods; multi-inlet microfluidic devices for precise content manipulation; period tunability reduced by the inhibition of positive feedback; cell cycle responses to endothall, okadaic acid, IPP2-His, and IPP2-GST; cell cycle responses to fostriecin and okadaic acid; polymorphic response to PP2A inhibition caused by interlinked bistable switches; and bifurcation analysis when tuning OA concentration (PDF)

Desynchronization of oscillations in droplets over time (AVI)

Three-channel tuning of cyclin B and PD166285 in droplets (AVI)

Bimodal OA concentration ranges support oscillations (AVI)

■ AUTHOR INFORMATION

Corresponding Author

Qiong Yang − *Department of Biophysics, University of Michigan, Ann Arbor, Michigan 48109, United States;* orcid.org/0000-0002-2442-2094; Phone: +1 734 764 4669; Email: qiongy@umich.edu

Authors

Zhengda Li − *Department of Biophysics, University of Michigan, Ann Arbor, Michigan 48109, United States; Department of Chemical and Systems Biology, Stanford University School of Medicine, Stanford, California 94305, United States*

Shiyuan Wang − *Department of Biophysics, University of Michigan, Ann Arbor, Michigan 48109, United States*

Meng Sun − *Department of Biophysics, University of Michigan, Ann Arbor, Michigan 48109, United States*

Minjun Jin − *Department of Biophysics, University of Michigan, Ann Arbor, Michigan 48109, United States*

Daniel Khain − *Department of Biophysics, University of Michigan, Ann Arbor, Michigan 48109, United States*

Complete contact information is available at: https://pubs.acs.org/10.1021/acssynbio.3c00631

Author Contributions

Z.L., S.W., and M.S. contributed equally to this work. Z.L. and Q.Y. conceptualized the work; Z.L., S.W., and M.S. designed the devices and performed the formal analysis; Z.L., S.W., M.S., M.J., and D.K. performed the experiments; Z.L. performed computational and modeling work; and Z.L., S.W., M.S., and Q.Y. wrote the paper.

Notes

The authors declare no competing financial interest.

https://doi.org/10.1021/acssynbio.3c00631
ACS Synth. Biol. 2024, 13, 804−815

■ ACKNOWLEDGMENTS

We thank Dr. J.K. for the critical reading of the manuscript. We thank the Yang laboratory for helpful discussions. We thank the financial support from NSF (MCB #1817909; MCB #2218083), NIH (R01GM144584), and NIH (S10OD026825) for the Lighthouse HPC high-performance computing cluster at the University of Michigan.

■ REFERENCES

(1) Gilbert, D. A. The Nature of the Cell Cycle and the Control of Cell Proliferation. *Curr. Mod. Biol.* **1974**, *5* (4), 197−206.
(2) Almouzni, G.; Wolffe, A. P. Constraints on Transcriptional Activator Function Contribute to Transcriptional Quiescence during Early Xenopus Embryogenesis. *EMBO J.* **1995**, *14* (8), 1752−1765.
(3) Masui, Y.; Wang, P. Cell Cycle Transition in Early Embryonic Development of Xenopus Laevis. *Biol. Cell* **1998**, *90* (8), 537−548.
(4) Murray, A. W.; Kirschner, M. W. Dominoes and Clocks: The Union of Two Views of the Cell Cycle. *Science* **1989**, *246* (4930), 614−621.
(5) KEGG PATHWAY: Cell cycle—Xenopus laevis (African clawed frog). https://www.genome.jp/pathway/xla04110 (accessed Oct 12, 2023).
(6) Novak, B.; Tyson, J. J. Modeling the Cell Division Cycle: M-Phase Trigger, Oscillations, and Size Control. *J. Theor. Biol.* **1993**, *165* (1), 101−134.
(7) Thron, C. D. A Model for a Bistable Biochemical Trigger of Mitosis. *Biophys. Chem.* **1996**, *57* (2−3), 239−251.
(8) Pomerening, J. R.; Sontag, E. D.; Ferrell, J. E. Building a Cell Cycle Oscillator: Hysteresis and Bistability in the Activation of Cdc2. *Nat. Cell Biol.* **2003**, *5* (4), 346−351.
(9) Novak, B.; Tyson, J. J. Numerical Analysis of a Comprehensive Model of M-Phase Control in Xenopus Oocyte Extracts and Intact Embryos. *J. Cell Sci.* **1993**, *106* (4), 1153−1168.
(10) Tyson, J. J.; Novák, B. Models in Biology: Lessons from Modeling Regulation of the Eukaryotic Cell Cycle. *BMC Biol.* **2015**, *13*, 46.
(11) Yang, Q.; Ferrell, J. E. The Cdk1-APC/C Cell Cycle Oscillator Circuit Functions as a Time-Delayed, Ultrasensitive Switch. *Nat. Cell Biol.* **2013**, *15* (5), 519−525.
(12) Tsai, T. Y.-C.; Choi, Y. S.; Ma, W.; Pomerening, J. R.; Tang, C.; Ferrell, J. E. Robust, Tunable Biological Oscillations from Interlinked Positive and Negative Feedback Loops. *Science* **2008**, *321* (5885), 126−129.
(13) Krasinska, L.; Domingo-Sananes, M. R.; Kapuy, O.; Parisis, N.; Harker, B.; Moorhead, G.; Rossignol, M.; Novák, B.; Fisher, D. Protein Phosphatase 2A Controls the Order and Dynamics of Cell-Cycle Transitions. *Mol. Cell* **2011**, *44* (3), 437−450.
(14) Mochida, S.; Rata, S.; Hino, H.; Nagai, T.; Novák, B. Two Bistable Switches Govern M Phase Entry. *Curr. Biol.* **2016**, *26* (24), 3361−3367.
(15) Rata, S.; Suarez Peredo Rodriguez, M. F.; Joseph, S.; Peter, N.; Echegaray Iturra, F.; Yang, F.; Madzvamuse, A.; Ruppert, J. G.; Samejima, K.; Platani, M.; Alvarez-Fernandez, M.; Malumbres, M.; Earnshaw, W. C.; Novak, B.; Hochegger, H. Two Interlinked Bistable Switches Govern Mitotic Control in Mammalian Cells. *Curr. Biol.* **2018**, *28* (23), 3824.
(16) Kamenz, J.; Gelens, L.; Ferrell, J. E. Bistable, Biphasic Regulation of PP2A-B55 Accounts for the Dynamics of Mitotic Substrate Phosphorylation. *Curr. Biol.* **2021**, *31* (4), 794.
(17) Guan, Y.; Li, Z.; Wang, S.; Barnes, P. M.; Liu, X.; Xu, H.; Jin, M.; Liu, A. P.; Yang, Q. A Robust and Tunable Mitotic Oscillator in Artificial Cells. *eLife* **2018**, *7*, No. e33549.
(18) Guan, Y.; Wang, S.; Jin, M.; Xu, H.; Yang, Q. Reconstitution of Cell-Cycle Oscillations in Microemulsions of Cell-Free *Xenopus* Egg Extracts. *J. Vis. Exp.* **2018**, *139*, e58240.
(19) Sun, M.; Li, Z.; Wang, S.; Maryu, G.; Yang, Q. Building Dynamic Cellular Machineries in Droplet-Based Artificial Cells with Single-Droplet Tracking and Analysis. *Anal. Chem.* **2019**, *91* (15), 9813−9818.
(20) Cao, Y.; Wang, H.; Ouyang, Q.; Tu, Y. The Free Energy Cost of Accurate Biochemical Oscillations. *Nat. Phys.* **2015**, *11* (9), 772−778.
(21) Weitz, M.; Kim, J.; Kapsner, K.; Winfree, E.; Franco, E.; Simmel, F. C. Diversity in the Dynamical Behaviour of a Compartmentalized Programmable Biochemical Oscillator. *Nat. Chem.* **2014**, *6* (4), 295−302.
(22) Hartley, R. S.; Rempel, R. E.; Maller, J. L. In Vivo Regulation of the Early Embryonic Cell Cycle in Xenopus. *Dev. Biol.* **1996**, *173* (2), 408−419.
(23) Maryu, G.; Yang, Q. Nuclear-Cytoplasmic Compartmentalization of Cyclin B1-Cdk1 Promotes Robust Timing of Mitotic Events. *Cell Rep.* **2022**, *41* (13), 111870.
(24) Araujo, A. R.; Gelens, L.; Sheriff, R. S. M.; Santos, S. D. M. Positive Feedback Keeps Duration of Mitosis Temporally Insulated from Upstream Cell-Cycle Events. *Mol. Cell* **2016**, *64* (2), 362−375.
(25) Goldbeter, A.; Koshland, D. E. An Amplified Sensitivity Arising from Covalent Modification in Biological Systems. *Proc. Natl. Acad. Sci. U.S.A.* **1981**, *78* (11), 6840−6844.
(26) Panek, R. L.; Lu, G. H.; Klutchko, S. R.; Batley, B. L.; Dahring, T. K.; Hamby, J. M.; Hallak, H.; Doherty, A. M.; Keiser, J. A. In Vitro Pharmacological Characterization of PD 166285, a New Nanomolar Potent and Broadly Active Protein Tyrosine Kinase Inhibitor. *J. Pharmacol. Exp. Ther.* **1997**, *283* (3), 1433−1444.
(27) Wlodarchak, N.; Xing, Y. PP2A as a Master Regulator of the Cell Cycle. *Crit. Rev. Biochem. Mol. Biol.* **2016**, *51* (3), 162−184.
(28) Bialojan, C.; Takai, A. Inhibitory Effect of a Marine-Sponge Toxin, Okadaic Acid, on Protein Phosphatases. Specificity and Kinetics. *Biochem. J.* **1988**, *256* (1), 283−290.
(29) Nordick, B.; Yu, P. Y.; Liao, G.; Hong, T. Nonmodular Oscillator and Switch Based on RNA Decay Drive Regeneration of Multimodal Gene Expression. *Nucleic Acids Res.* **2022**, *50* (7), 3693−3708.
(30) Li, Z.; Liu, S.; Yang, Q. Incoherent Inputs Enhance the Robustness of Biological Oscillators. *Cell Syst.* **2017**, *5* (1), 72.

https://doi.org/10.1021/acssynbio.3c00631
ACS Synth. Biol. 2024, 13, 804−815